Available online at www.sciencedirect.com

ScienceDirect

IFAC Papers Online CONFERENCE PAPER ARCHIVE

IFAC PapersOnLine 52-12 (2019) 176–181

Linear Quadratic Regulator for Trajectory Tracking of a Quadrotor

Luís Martins[2] **Carlos Cardeira**[1,2] **Paulo Oliveira**[1,2]

[1] IDMEC, [2] Instituto Superior Técnico, Universidade de Lisboa, Portugal

{luis.cunha.martins, carlos.cardeira, paulo.j.oliveira}@tecnico.ulisboa.pt

Abstract: In this paper, an inner-outer loop control structure with linear quadratic optimal controllers and integrative action is proposed for trajectory tracking of an Unmanned Aerial Vehicle. The dynamic model of the quadrotor is derived and linearized in preparation for the design of the controllers. The full state-feedback relies on measurements from motion sensors installed on-board and on on-flight estimates provided by Kalman filters and an attitude filter. The control system obtained is validated in simulation and implemented in a commercially available drone, equipped with an Inertial Measurement Unit, a compass and an altimeter. The inertial position of the drone is given by a motion capture system.

Keywords: Trajectory-Tracking, Inner-Outer Loop, Linear Control, Integrative Action

1. INTRODUCTION

In recent years, the popularity of drones has increased immensely as the embedded technology advanced. This growth translated into an intensive study of these Unmanned Aerial Vehicles. Its maneuverability, hovering capabilities, reduced price and small size not only enables the quadrotors to be equated in a wide range of applications, such as infrastructure inspection or area monitoring, but also constitutes them as an excellent alternative for the experimentation of control and navigation techniques. At the core of the development of these applications, a robust control structure and an in-flight state-estimation is required.

The study of the control of quadrotors is vast and includes diverse linear and nonlinear techniques. Concerning the linear approach, the majority of the bibliography reports the application of classical PIDs control and modern LQR controllers. In Bouabdallah et al. (2004) a comparison between the performances of the classical and the modern controllers referred, in simulation and in flight, for attitude control is established. This work evidences that the non-inclusion of an integrative action in LQR control for attitude originates a steady-state error. Bauer and Bokor (2008) implemented an LQ servo controller with a double integrator for trajectory tracking in simulation and Sabatino (2015) developed the same but without the integrative action. Lastly, an inner and outer control loop with LQR control with integration action is proposed by Raja (2017). This control structure, designed for a model of a quadrotor obtained through Jacobian linearization, is successfully implemented in a UAV and enables a more effective attitude response.

In this paper, a linearized model of the quadcopter is derived for the hover position in order to enable the implementation of linear controllers. The reconstruction of the state variables that are not directly available through sensors is performed resorting to Kalman Filters and the attitude filter proposed by Madgwick et al. (2011). An inner-outer loop control structure is implemented, where the innermost loop is responsible for the attitude control and the outermost solves the positioning control. In both loops an integrative action is present. To tackle the control problem, the LQR approach is considered.

The main contributions of this paper are: the derivation of a simplified dynamic model for quadrotors with X configuration, the subsequent linearization for trim position and the application of model-based LQR control with integrative action in an inner-outer loop structure that is validated in simulation and in a real system.

This paper is organized as follows: the physical model and the subsequent linearization are detailed in section 2; in section 3, the state-estimation is addressed; the control architecture and design is presented in section 4; the simulation results obtained with the simplified nonlinear model and the control structure designed are discussed in section 5; the quadcopter model and its sensors are detailed and the implementation of the controllers is described in section 6; experimental results are presented and analyzed in section 7; finally, some concluding remarks are drawn.

2. PHYSICAL MODEL

2.1 Nonlinear Model

In this section, the nonlinear model of the UAV based on the Newton-Euler formalism is presented. The nonlinear dynamics are described in the body-fixed $\{B\}$ and in the inertial $\{I\}$ frames, depicted in Fig. 1. The unit vectors along the axis of the body-fixed frame are denoted by $\{\vec{b}_1, \vec{b}_2, \vec{b}_3\}$ and the unit vector along the inertial frame $\{I\}$ axis are denoted by $\{\vec{a}_1, \vec{a}_2, \vec{a}_3\}$. It is assumed that the origin of the body-fixed frame $\{B\}$ is coincident with the center of mass of the quadrotor.

10.1016/j.ifacol.2019.11.195

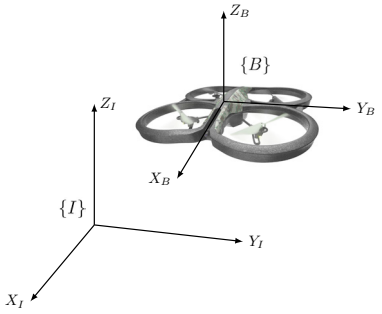

Fig. 1. Reference frames in which the nonlinear dynamics are described.

Let $\mathbf{p} = [x\ y\ z]^T$ denote the position vector of the center of mass of the UAV in the inertial frame. Let $\boldsymbol{\eta} = [\varphi\ \theta\ \psi]^T$ describe the orientation vector, in terms of Euler angles, of the body-fixed frame with respect to the inertial frame, where φ, θ and ψ are the roll, pitch and yaw angles, respectively. Let $\boldsymbol{\omega} = [p\,q\,r]^T$ represent the angular velocity described in the reference frame $\{B\}$. The rigid body equations of motion of the quadcopter according to Mahony et al. (2012) are given by:

$$m\ddot{\mathbf{p}} = -mg\vec{a}_3 + {}^I\mathbf{R}_B\mathbf{F} \tag{1}$$

$$\mathbf{I}\dot{\boldsymbol{\omega}} = -\boldsymbol{\omega} \times \mathbf{I}\boldsymbol{\omega} + \boldsymbol{\tau} \tag{2}$$

where $\mathbf{I}$ corresponds to the 3×3 constant inertia matrix described in the body fixed-frame, m is the total mass of the quadrotor, g denotes the gravity acceleration, $\mathbf{F}$ and $\boldsymbol{\tau}$ denote, respectively, the principal forces and moments applied to UAV by the aerodynamics of the rotors, both described in the reference frame $\{B\}$, and ${}^I\mathbf{R}_B$ is the rotation matrix from the body-fixed to the inertial frame. Note that the axis convention used is different than the one Mahony et al. (2012) considered. The Euler angles follow the sequence of rotation Z-Y-X that is described in Oriolo et al. (2010). The resultant rotation matrix is given by:

$${}^I\mathbf{R}_B = \begin{bmatrix} c_\theta c_\psi & s_\varphi s_\theta c_\psi - c_\varphi s_\psi & c_\varphi s_\theta c_\psi + s_\varphi s_\psi \\ c_\theta s_\psi & s_\varphi s_\theta s_\psi - c_\varphi c_\psi & c_\varphi s_\theta s_\psi - s_\varphi c_\psi \\ -s_\theta & s_\varphi c_\theta & c_\varphi c_\theta \end{bmatrix} \tag{3}$$

where c and s are the shorthand forms for cosine and sine, respectively.

The angle rates $\dot{\boldsymbol{\eta}} = [\dot{\varphi}\ \dot{\theta}\ \dot{\psi}]^T$ are obtained from the body rotational rates using the following system of equations:

$$\begin{bmatrix} \dot{\varphi} \\ \dot{\theta} \\ \dot{\psi} \end{bmatrix} = \begin{bmatrix} 1 & \sin(\varphi)\tan(\theta) & \cos(\varphi)\tan(\theta) \\ 0 & \cos(\varphi) & -\sin(\varphi) \\ 0 & \sin(\varphi)\sec(\theta) & \cos(\varphi)\sec(\theta) \end{bmatrix} \begin{bmatrix} p \\ q \\ r \end{bmatrix} \tag{4}$$

According to Leishman (2000), the steady-state thrust T_i and yaw moment τ_{ψ_i} generated by rotor i in free air can be modeled as follow:

$$T_i = c_{T_i}\Omega_i^2 \tag{5}$$

$$\tau_i = c_{\tau_i}\Omega_i^2 \tag{6}$$

where c_{T_i} and c_{τ_i} are coefficients possible to determine experimentally that are dependent on the area of the disk, the radius of the rotor, the density of air, the geometry and the profile of the rotor, and the effect of drag by the rotor flow. Therefore, the relation between the generated yaw moment τ_{ψ_i} by a rotor and its generated thrust T_i is described by the following expression:

$$\tau_{\psi_i} = \frac{c_{\tau_i}}{c_{T_i}}T_i = c_i T_i \tag{7}$$

The roll and pitch moments, τ_φ and τ_θ, result from the generated thrust of the rotor and its arrangement relative to the center of mass of the quadcopter. Hence, the resultant total thrust T and moments τ_φ, τ_θ and τ_ψ, for a quadrotor with a *X-configuration*, are computed through:

$$\begin{bmatrix} T \\ \tau_\varphi \\ \tau_\theta \\ \tau_\psi \end{bmatrix} = \begin{bmatrix} 1 & 1 & 1 & 1 \\ L & -L & -L & L \\ -L & -L & L & L \\ c_1 & -c_2 & c_3 & -c_4 \end{bmatrix} \begin{bmatrix} T_1 \\ T_2 \\ T_3 \\ T_4 \end{bmatrix} \tag{8}$$

where L denotes the perpendicular distance of the rotor to the x or y axis of the body-fixed frame, as the case may be.

There are various aerodynamic and gyroscopic effects associated with the rotors craft that increase the complexity of the model. However, a model with such level of precision is not required, not only because the control can overcome these secondary effects according to Mahony et al. (2012), but also due to the fact that is widely shown in the literature that the control can achieve high performance with the simplified model of the rotor. Consequently, high order effects such as *blade flapping*, *aerodynamic drag*, *translational lift* and *vortex states* caused by axial motion are neglected. Furthermore, it is assumed that the total thrust generated T is oriented along the $\vec{b}_3$ direction, i.e., parallel to the axis of the rotor, and the coefficients of the rotor are constant (static thrust and moments).

Moreover, the quadrotor is assumed to be exactly symmetrical, which implies that the inertia matrix is diagonal, and the rotor gyroscopic effects are neglected. Additionally, since the UAV flies at a height higher than $0,50m$, except when the take-off or the landing occurs, the ground effect is ignored.

2.2 Linearized Model

The point of equilibrium for which the linearization will be deduced is the hover condition ($\mathbf{p} = [x\ y\ z]^T$, $\boldsymbol{\eta} = [0\ 0\ 0]^T$), where the yaw angle ψ is additionally considered zero. Note that the linearization could be performed for other conditions, however, this one was chosen given its simplicity. By resorting to the Taylor series till the first order term enables to approximate the cosine of the Euler angles to 1 and the sine and tangent of the referred angles to the angle itself.

For the *height subsystem*, the differential equation simplifies into:

$$\ddot{z} \cong \frac{1}{m}(T - mg) \tag{9}$$

Defining the following state variables and modified input of the subsystem,

$$\mathbf{x_z} = [z\ \dot{z}]^T,\ \mathbf{u_z} = T - mg \tag{10}$$

leads to the state-space representation described below:

$$\dot{\mathbf{x}}_\mathbf{z} = \begin{bmatrix} 0 & 1 \\ 0 & 0 \end{bmatrix}\mathbf{x_z} + \begin{bmatrix} 0 \\ 1/m \end{bmatrix}\mathbf{u_z} \tag{11}$$

$$\mathbf{y_z} = [1\ 0]\,\mathbf{x_z} \tag{12}$$

The variation of the position of the UAV along the x and y directions of the inertial frame is a direct result of the variation of pitch and roll angles, respectively. The linearization of the second derivative of the pitch angle yields:

$$\ddot{\theta} \cong \frac{\tau_\theta}{I_y} \tag{13}$$

Defining the consequent state variables and modified input of the subsystem,

$$\mathbf{x_\theta} = [\theta\ \dot{\theta}]^T,\ \mathbf{u_\theta} = \tau_\theta \tag{14}$$

results in the state-space representation described below:

$$\dot{\mathbf{x}}_{\boldsymbol{\theta}} = \begin{bmatrix} 0 & 1 \\ 0 & 0 \end{bmatrix} \mathbf{x}_{\boldsymbol{\theta}} + \begin{bmatrix} 0 \\ 1/I_y \end{bmatrix} \mathbf{u}_{\boldsymbol{\theta}} \tag{15}$$

$$\mathbf{y}_{\boldsymbol{\theta}} = [1\ 0]\, \mathbf{x}_{\boldsymbol{\theta}} \tag{16}$$

The linearization of the second derivative of the roll angle results in:

$$\ddot{\varphi} \cong \frac{\tau_\varphi}{I_x} \tag{17}$$

Letting the following equations define the state variables and modified input of the subsystem

$$\mathbf{x_\varphi} = [\varphi\ \dot{\varphi}]^T,\ \mathbf{u_\varphi} = \tau_\varphi \tag{18}$$

the obtained state-space representation is described by

$$\dot{\mathbf{x}}_{\boldsymbol{\varphi}} = \begin{bmatrix} 0 & 1 \\ 0 & 0 \end{bmatrix} \mathbf{x}_{\boldsymbol{\varphi}} + \begin{bmatrix} 0 \\ 1/I_x \end{bmatrix} \mathbf{u}_{\boldsymbol{\varphi}} \tag{19}$$

$$\mathbf{y}_{\boldsymbol{\varphi}} = [1\ 0]\, \mathbf{x}_{\boldsymbol{\varphi}} \tag{20}$$

The acceleration in the body-fixed frame vector, ${}^B\mathbf{a}$, is given by

$${}^B\mathbf{a} = \frac{\mathbf{F}}{m} - {}^B\mathbf{R}_I g \overrightarrow{a_3} - \boldsymbol{\omega} \times {}^B\mathbf{v} \tag{21}$$

where ${}^B\mathbf{v}$ denotes the velocities in the body-fixed frame and the term $\boldsymbol{\omega} \times {}^B\mathbf{v}$ corresponds to the centripetal acceleration. The accelerations along the x axis, ${}^B\mathbf{a}_x$, and along the y axis, ${}^B\mathbf{a}_y$, of the body-fixed frame, after being linearized and assuming that the yaw angle ψ is kept at zero and that the movement along the body fixed-frame x and y directions occurs with negligible variations along the z direction, are equal to

$${}^B\mathbf{a}_x = \theta g \tag{22}$$

$${}^B\mathbf{a}_y = -\varphi g \tag{23}$$

Noticing that the forward velocity of the UAV in the body-fixed frame, u, is the integral of ${}^B\mathbf{a}_x$, and the sideway velocity, v, is the integral of ${}^B\mathbf{a}_y$ the equations 22 and 23 can be rewritten as

$$\dot{u} = \theta g \tag{24}$$

$$\dot{v} = -\varphi g \tag{25}$$

With the establishment of the next state-variables and modified input of the subsystem:

$$\mathbf{x_x} = [{}^B x_I\ u]^T,\ \mathbf{u_x} = \theta \tag{26}$$

where ${}^B x_I$ denotes the x coordinate of the inertial position described according to the orientation of the body-fixed frame, the following state-space representation, that relates the ${}^B x_I$ coordinate of the position with the pitch angle, θ, is obtained

$$\dot{\mathbf{x}}_{\mathbf{x}} = \begin{bmatrix} 0 & 1 \\ 0 & 0 \end{bmatrix} \mathbf{x}_{\mathbf{x}} + \begin{bmatrix} 0 \\ g \end{bmatrix} \mathbf{u}_{\mathbf{x}} \tag{27}$$

$$\mathbf{y}_{\mathbf{x}} = [1\ 0]\, \mathbf{x}_{\mathbf{x}} \tag{28}$$

By defining the following state-variables and modified input of the subsystem:

$$\mathbf{x_y} = [{}^B y_I\ v]^T,\ \mathbf{u_y} = \varphi \tag{29}$$

where ${}^B y_I$ denotes the y coordinate of the inertial position described according to the orientation of the body-fixed, the following state-space representation, that relates this coordinate of the position with the roll angle, φ, is obtained

$$\dot{\mathbf{x}}_{\mathbf{y}} = \begin{bmatrix} 0 & 1 \\ 0 & 0 \end{bmatrix} \mathbf{x}_{\mathbf{y}} + \begin{bmatrix} 0 \\ -g \end{bmatrix} \mathbf{u}_{\mathbf{y}} \tag{30}$$

$$\mathbf{y}_{\mathbf{y}} = [1\ 0]\, \mathbf{x}_{\mathbf{y}} \tag{31}$$

The linearization of the second derivative of the yaw angle yields:

$$\ddot{\psi} \cong \frac{\tau_\psi}{I_z} \tag{32}$$

Letting the state-variables and entry of the subsystem be described by

$$\mathbf{x_\psi} = [\psi\ \dot{\psi}]^T,\ \mathbf{u_\psi} = \tau_\psi \tag{33}$$

enables the following state-space representation

$$\dot{\mathbf{x}}_{\boldsymbol{\psi}} = \begin{bmatrix} 0 & 1 \\ 0 & 0 \end{bmatrix} \mathbf{x}_{\boldsymbol{\psi}} + \begin{bmatrix} 0 \\ 1/I_z \end{bmatrix} \mathbf{u}_{\boldsymbol{\psi}} \tag{34}$$

$$\mathbf{y}_{\boldsymbol{\psi}} = [1\ 0]\, \mathbf{x}_{\boldsymbol{\psi}} \tag{35}$$

3. STATE-ESTIMATION

3.1 Attitude Filter

The Kalman filter is widely used for sensor fusion to estimate the attitude, however, for practical reasons, the orientation filter developed by Madgwick et al. (2011) was opted instead, due to its reduced computational effort. The computation is performed using the quaternion representation and fuses the measurements of the gyroscope, accelerometer and magnetometer through an optimized gradient-descent algorithm.

3.2 Kalman Filter

This filter, with a statistical basis, constitutes a solution to optimal stochastic estimation for linear systems and aims the minimization of the estimation mean squared error, under the assumptions of zero-mean Gaussian process and sensor noises, w and α, respectively, as proposed by Kalman (1960). For the estimation of the velocities the following observable subsystem with noise disturbances was considered:

$$\dot{\mathbf{x}} = \begin{bmatrix} 0 & 1 \\ 0 & 0 \end{bmatrix} \mathbf{x} + w \tag{36}$$

$$\mathbf{y} = [1\ 0]\, \mathbf{x} + \alpha \tag{37}$$

where the first state-variable is one of the inertial coordinates (x, y, z), whose measurements are available through sensors, and the second state-variable is the respective inertial velocity $(\dot{x}, \dot{y}, \dot{z})$. The estimates for the body-fixed velocities u and v are obtained by applying the following rotation:

$$\begin{bmatrix} \hat{u} \\ \hat{v} \end{bmatrix} = {}^B\mathbf{R}_{I_{ij}} \begin{bmatrix} \hat{\dot{x}} & \hat{\dot{y}} & \hat{\dot{z}} \end{bmatrix}^T,\ i \in \{1, 2\}, j \in \{1, 2, 3\} \tag{38}$$

4. CONTROL

The Linear Quadratic Regulator is an optimal controller that uses full state-feedback and is derived as a solution to an optimization process where the system dynamics imposes the restrictions. For a system described by the state-space representation

$$\dot{\mathbf{x}} = \mathbf{A}\mathbf{x} + \mathbf{B}\mathbf{u} \tag{39}$$

$$\dot{\mathbf{y}} = \mathbf{C}\mathbf{x} + \mathbf{D}\mathbf{u} \tag{40}$$

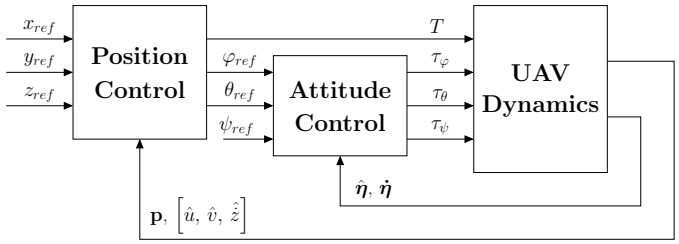

Fig. 2. Scheme of the inner-outer loop control structure implemented.

the optimal regulator problem determines the gain matrix $\mathbf{K}$, constituent of the optimal control vector

$$\mathbf{u}(t) = -\mathbf{K}\mathbf{x}(t) \tag{41}$$

that ensures the minimization of the performance index

$$J = \int_0^\infty (\mathbf{x}^T\mathbf{Q}\mathbf{x} + \mathbf{u}^T\mathbf{R}\mathbf{u})dt \tag{42}$$

where the first quadratic form includes the real symmetric state weighting matrix $\mathbf{Q}$ and the second quadratic term comprises the real symmetric control weighting matrix $\mathbf{R}$.

The computation of the optimal gains is performed through:

$$\mathbf{K} = \mathbf{R}^{-1}\mathbf{B}^T\mathbf{P} \tag{43}$$

where the positive-definite matrix $\mathbf{P}$ results from the steady-state Riccati equation:

$$\mathbf{A}^T\mathbf{P} + \mathbf{P}\mathbf{A} - \mathbf{P}\mathbf{B}\mathbf{R}^{-1}\mathbf{B}^T\mathbf{P} + \mathbf{Q} = 0 \tag{44}$$

As a way of dealing with the effect of perturbations and with the steady-state error, an integrator was embedded in the control structure. This inclusion leads to additional robustness of the control system and eliminates the steady-state errors due to constant disturbances. Let the reference signal be represented by $\mathbf{r}$ and the difference between the output of the system, $\mathbf{y}$, and the reference, $\mathbf{r}$, be the time derivative of the state-space variable that results from adding the referred integrator, $\boldsymbol{\xi}$. The matrices of the resulting regulator are given by

$$\bar{\mathbf{A}} = \begin{bmatrix} \mathbf{A} & \mathbf{0} \\ -\mathbf{C} & \mathbf{0} \end{bmatrix}, \bar{\mathbf{B}} = \begin{bmatrix} \mathbf{B} \\ \mathbf{0} \end{bmatrix} \tag{45}$$

The optimal gains are computed by directly applying the LQR gain computation presented formerly. The optimal gain matrix obtained

$$\bar{\mathbf{K}} = [\mathbf{K} \ -\mathbf{k_1}] \tag{46}$$

is constituted by the vector of gains for the state-variables, $\mathbf{K}$, and by the gain for the integrative action, $\mathbf{k_1}$.

The specifications desired for the UAV position are the absence of overshoot and null steady-error when the system is subjected to a constant input. Regarding the attitude loop, once is responsible for the stabilization of the UAV, it must be much faster to cope with the references that result from the translational control in the x and y directions of the inertial frame. Therefore, the pitch θ and roll φ subsystems are required to present time responses with a settling time lower than one second and a null steady-state error. Considering the yaw ψ subsystem, since it does not have such an important role in the stabilization of the drone as the other Euler angles and, also, because an excessively aggressive response could impact the other subsystems when this one is subjected to perturbations, it is not required for its response to share such characteristics apart from the null steady-state error.

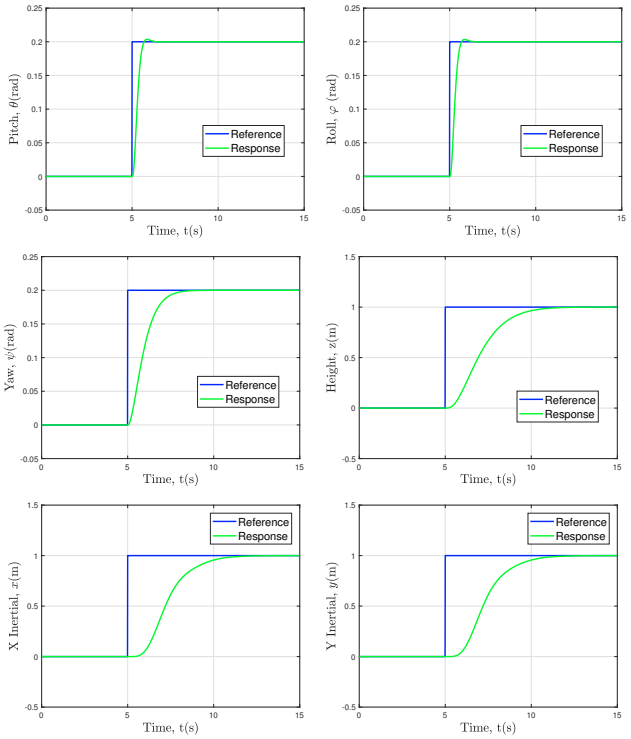

Fig. 3. Step-responses obtained in simulation with the controllers designed. From left to right, top to bottom: (a) Pitch; (b) Roll; (c) Yaw; (d) Height; (e) X Inertial and (f) Y Inertial.

Table 1. $\mathbf{Q}$ and $\mathbf{R}$ matrices used in the optimal gains computation for each subsystem

Subsystem	Q	R
Pitch	diag(25, 1, 1500)	200
Roll	diag(25, 1, 1500)	200
Yaw	diag(7, 1, 15)	1
X Position	diag(15, 1, 10)	1000
Y Position	diag(15, 1, 10)	1000
Height	diag(5, 1, 3)	3

The resulting step-responses, obtained with the $\mathbf{Q}$ and $\mathbf{R}$ matrices detailed in Table. 1, are depicted in Fig. 3.

5. SIMULATION RESULTS

To evaluate the performances of the proposed control architecture, a trajectory was created and given as a reference for the subsystems. Additionally, noise disturbances, modeled as zero-mean Gaussian white noise, were included to study the impact of the noise of the sensors. This trajectory is defined with a constant yaw angle equal to zero and, excluding the take-off, is formed by rectilinear sections, with a constant velocity of $0.05\ \mathrm{m} \cdot \mathrm{s}^{-1}$, and semicircular sections, with a constant angular velocity of $0.05\pi\ \mathrm{rad} \cdot \mathrm{s}^{-1}$.

From the observation of the Fig. 4, it can be concluded that the control structure implemented allows a good following of the trajectory. The time responses have a steady-state error for references with constant velocity, which was predictable since the integrator included in the control structure only has the capacity to eliminate the steady-state error for constant references. Notwithstanding, once the ramp references are followed up by constant

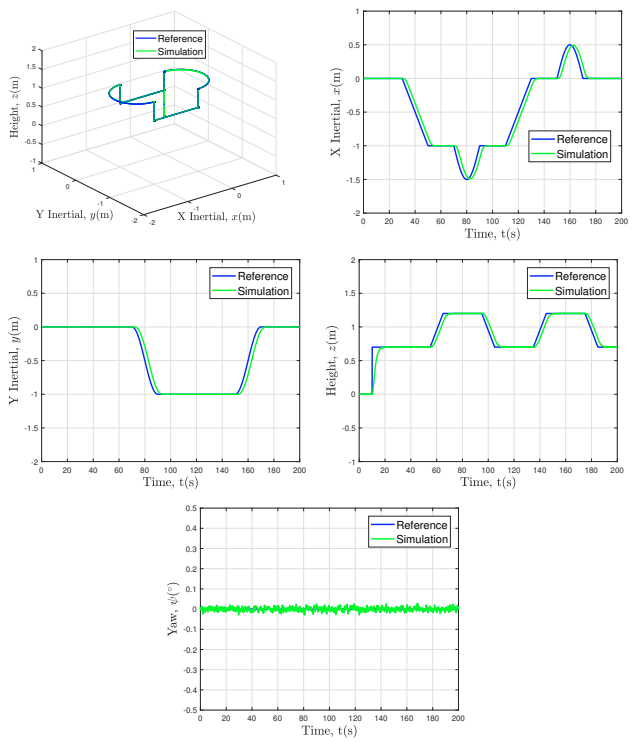

Fig. 4. Responses obtained during trajectory tracking in simulation. From left to right, top to bottom: (a) Trajectory Tracking in 3D space; (b) X Inertial; (c) Y Inertial; (d) Height and (e) Yaw.

references, the responses converge without error to the desired coordinate. Concerning the time response of the yaw angle, it is visible that the purpose was achieved inasmuch as the module did not exceed one-hundredth of degree.

6. IMPLEMENTATION

The Parrot AR. Drone 2.0 was selected as the unmanned aerial vehicle used for testing the proposed control system solution. This commercially available quadcopter possesses an inboard Inertial Measurement Unit and a sonar board. The IMU is constituted by a 3-axis accelerometer, a 3-axis gyroscope and a barometric pressure sensor. The sonar board is equipped with two ultrasonic transducers and a 3-axis Compass. These sensors provide measurements of the acceleration, of the angular velocities, of the UAVs height and of the magnetic field. The inertial position of the vehicle is provided by a motion capture system.

In order to implement the control structure in the quadrotor, the "AR Drone 2.0 Quadcopter Embedded Coder" developed by Lee (2016) was used. This *Simulink* project enables direct access to the sensors and the actuators of the quadcopter.

The Pulse Width Modulation Commands for the actuators are computed from the Thrust and Moments, that result from the control law, through experimentally determined relations. For further details see Martins (2019). The relevant physical quantities of this quadcopter are detailed in Table. 2

Table 2. Important physical quantities of the AR Drone 2.0.

L (m)	m (kg)	I_x (kg · m^2)	I_y (kg · m^2)	I_z (kg · m^2)
0.127	0.460	2.24×10^{-3}	2.90×10^{-3}	5.30×10^{-3}

7. EXPERIMENTAL RESULTS

The experimental results are depicted in Fig. 5. The trajectory tested is equal to the simulated one and it is possible to verify a good tracking by the quadrotor. It is important to stress that: the take-off is present in the results depicted, the altimeter does not measure heights inferior to 30 cm and that a heavier battery was used leading to higher values of thrust. Nonetheless, despite this change in the total mass of the UAV, the results did not deteriorate since the integral action was included. The controllers had to be adjusted when implemented in the UAV. The matrices **Q** and **R** used in this adjustment are detailed in Table. 3.

Table 3. **Q** and **R** matrices used in the adjustment of the controllers implemented in the UAV

Subsystem	**Q**	**R**
Yaw	diag(18, 2, 2)	30
X Position	diag(3, 1, 2)	300
Y Position	diag(3, 1, 2)	500
Height	diag(3, 1, 1)	1

By comparing the UAV results with the simulation responses, the similarities between them are clear, which indicates that the nonlinear model considered possesses a satisfactory degree of proximity. The histograms of the absolute error for the inertial coordinates and the yaw angle during the tracking of the trajectory (initiates at 20 seconds) are presented in Fig. 5. Even though the deviations are larger in the real system, they are still considered reduced. The local maxima visible in the position histograms are a consequence of the static error in the following of ramp inputs. Nevertheless, the maximum instances of error for all of these coordinates correspond approximately to zero, which is symptomatic of the capacity of the control system to maintain these coordinates at a constant value. The inertial coordinate x presented the higher deviations, which was expected since that was the subsystem more solicited. The values of the yaw angle obtained demonstrate that the goal defined for this Euler angle was achieved.

Table 4. Root-mean-square error in Simulation and in the UAV.

	x (m)	y (m)	z (m)	ψ (°)
Simulation	0.0865	0.0714	0.0556	0.0095
Experimental	0.1010	0.0781	0.0570	0.2244

The root-mean-square error for the trajectory tracking in simulation an in the real system is detailed in Table. 4. The height response obtained with the quadrotor has almost the same error obtained in simulation, whereas the other subsystems showed a forecastable increase in the real system due to the discarding of the higher order dynamics effects. In general, the errors were kept under reasonable values with the transition to the drone.

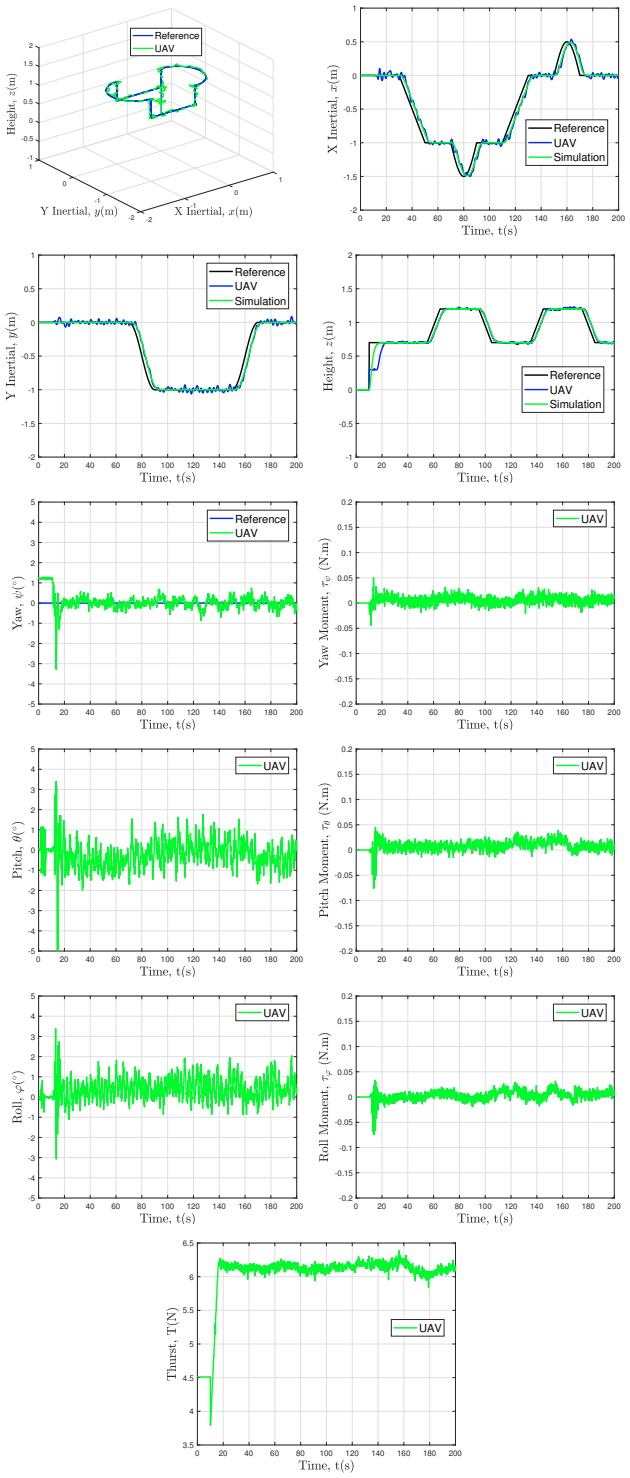

Fig. 5. Responses and actuations obtained during trajectory tracking with the UAV. From left to right, top to bottom: (a) Trajectory Tracking in 3D space; (b) X Inertial; (c) Y Inertial; (d) Height (e) Yaw; (f) Yaw Moment; (g) Pitch; (h) Pitch Moment; (i) Roll; (j) Roll Moment and (k) Thrust.

8. CONCLUSION

The dynamic model of the UAV considered proved to be accurate and sufficient, even though higher order effects were neglected. The inner-outer loop control structure, constituted by linear quadratic controllers whose design relying on the linearization of the referred model, provided good results in trajectory tracking, presenting robustness to perturbations not only in simulation but also in the real system.

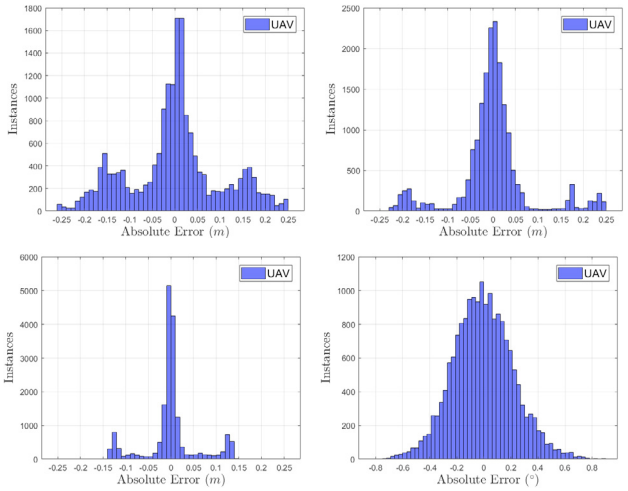

Fig. 6. Absolute Error Histograms. Left to right, top to bottom: (a) X Inertial; (b) Y Inertial; (c) Height and (d) Yaw.

9. ACKNOWLEDGEMENTS

This work was supported by FCT, through IDMEC, under LAETA, project UID/EMS/50022/2019.

REFERENCES

Bauer, P. and Bokor, J. (2008). Lq servo control design with kalman filter for a quadrotor uav. *Periodica Polytechnica Transportation Engineering*, 36(1-2), 9–14.

Bouabdallah, S., Noth, A., and Siegwart, R. (2004). Pid vs lq control techniques applied to an indoor micro quadrotor. *IEEE/RSJ International Conference on Intelligent Robots and Systems (IROS)*, 3, 2451–2456.

Kalman, R.E. (1960). A new approach to linear filtering and prediction problems. *Journal of Basic Engineering*, 82(1), 35–45.

Lee, D. (2016). Ar.drone 2.0 support from embedded coder. URL `https://www.mathworks.com/hardware-support/ar-drone.html`.

Leishman, J.G. (2000). *Principles of helicopter aerodynamics*. Cambridge University Press.

Madgwick, S.O.H., Harrison, A.J.L., and Vaidyanathan, R. (2011). Estimation of imu and marg orientation using a gradient descent algorithm. In *2011 IEEE International Conference on Rehabilitation Robotics*, 1–7.

Mahony, R., Kumar, V., and Corke, P. (2012). Multirotor aerial vehicles: Modeling, estimation, and control of quadrotor. *IEEE Robotics Automation Magazine*, 19(3), 20–32.

Martins, L. (2019). *Linear and Nonlinear Control of UAVs: Design and Experimental Validation*. Master's thesis, Instituto Superior Técnico, Lisbon, Portugal.

Oriolo, G., Sciavicco, L., Siciliano, B., and Villani, L. (2010). *Robotics: Modelling, Planning and Control*. Springer.

Raja, M. (2017). *Extended Kalman Filter and LQR controller design for quadrotor UAVs*. Master's thesis, Wright state University, Dayton,Ohio.

Sabatino, F. (2015). *Quadrotor control: modeling, nonlinear control design, and simulation*. Master's thesis, KTH Electrical Engineering, Stockholm.